J Seismol
DOI 10.1007/s10950-017-9704-y

ORIGINAL ARTICLE

Empirical equations for the prediction of PGA and pseudo spectral accelerations using Iranian strong-motion data

H. Zafarani · Lucia Luzi · Giovanni Lanzano · M. R. Soghrat

Received: 4 January 2016 / Accepted: 14 September 2017

Abstract A recently compiled, comprehensive, and good-quality strong-motion database of the Iranian earthquakes has been used to develop local empirical equations for the prediction of peak ground acceleration (PGA) and 5%-damped pseudo-spectral accelerations (PSA) up to 4.0 s. The equations account for style of faulting and four site classes and use the horizontal distance from the surface projection of the rupture plane as a distance measure. The model predicts the geometric mean of horizontal components and the vertical-to-horizontal ratio. A total of 1551 free-field acceleration time histories recorded at distances of up to 200 km from 200 shallow earthquakes (depth < 30 km) with moment magnitudes ranging from M_w 4.0 to 7.3 are used to perform regression analysis using the random effects algorithm of Abrahamson and Youngs (Bull Seism Soc Am 82:505–510, 1992), which considers between-events as well as within-events errors. Due to the limited data used in the development of previous Iranian ground motion prediction equations (GMPEs) and strong trade-offs between different terms of GMPEs, it is likely that the previously determined models might have less precision on their coefficients in comparison to the current study. The richer database of the current study allows improving on prior works by considering additional variables that could not previously be adequately constrained. Here, a functional form used by Boore and Atkinson (Earthquake Spect 24:99–138, 2008) and Bindi et al. (Bull Seism Soc Am 9:1899–1920, 2011) has been adopted that allows accounting for the saturation of ground motions at close distances. A regression has been also performed for the V/H in order to retrieve vertical components by scaling horizontal spectra. In order to take into account epistemic uncertainty, the new model can be used along with other appropriate GMPEs through a logic tree framework for seismic hazard assessment in Iran and Middle East region.

Keywords Ground motion prediction equations · Strong motion · PSHA · V/H ratio · Iran

1 Introduction

Ground motion prediction equations (GMPEs) make the core of any modern probabilistic seismic hazard analysis (PSHA). Currently, in the classical PSHA approach (McGuire 1978), the aleatory uncertainty, representing random variability of amplitudes about a median prediction equation, is handled using the principle assumption of normal distribution of

H. Zafarani (✉) · M. R. Soghrat
International Institute of Earthquake Engineering and Seismology (IIEES), No. 26, Arghavan St., North Dibajee, Farmanieh, P.O. Box: 19395/3913, Tehran, Iran
e-mail: h.zafarani@iiees.ac.ir

L. Luzi · G. Lanzano
Istituto Nazionale di Geofisica e Vulcanologia, Via Bassini 15, 20133 Milan, Italy

Published online: 12 October 2017

observations around the mean value predicted by GMPEs. Development of such equations considering local, regional, or global databases is an active and important area of research, though currently there are a large number of published ground-motion models in the literature (see, e.g., Douglas 2011). Cotton et al. (2006) and Bommer et al. (2010) have proposed some criteria for selection and ranking of appropriate GMPEs for practical applications. They have described in detail the criteria that should be used in order to avoid unintended subjectivity in the process of model selection before more elaborate data-testing methods. Currently, there is not a sound conclusion regarding the applicability of global relations to individual areas (e.g., Scasserra et al. 2009; Delavaud et al. 2012; Mousavi et al. 2012 and 2014; Zafarani and Mousavi 2014). Moreover, due to the complex forms of most of the global models, they are hardly implemented in the current practice of PSHA in Iran.

There are also some local GMPEs in Iran which have been developed in recent years. Zafarani et al. (2008), Soghrat et al. (2012), and Zafarani and Soghrat (2012) developed simulation or physics-based ground-motion prediction equations for Iran, northern Iran (including Alborz and Kopeh Dagh mountain ranges, see Fig. 1) and the Zagros fold belt, respectively, based on the specific barrier model (Halldorsson and Papageorgiou 2005) used within the context of the stochastic model. Ghasemi et al. (2009a) and Saffari et al. (2012) developed empirical models specifically for Iran. Neither

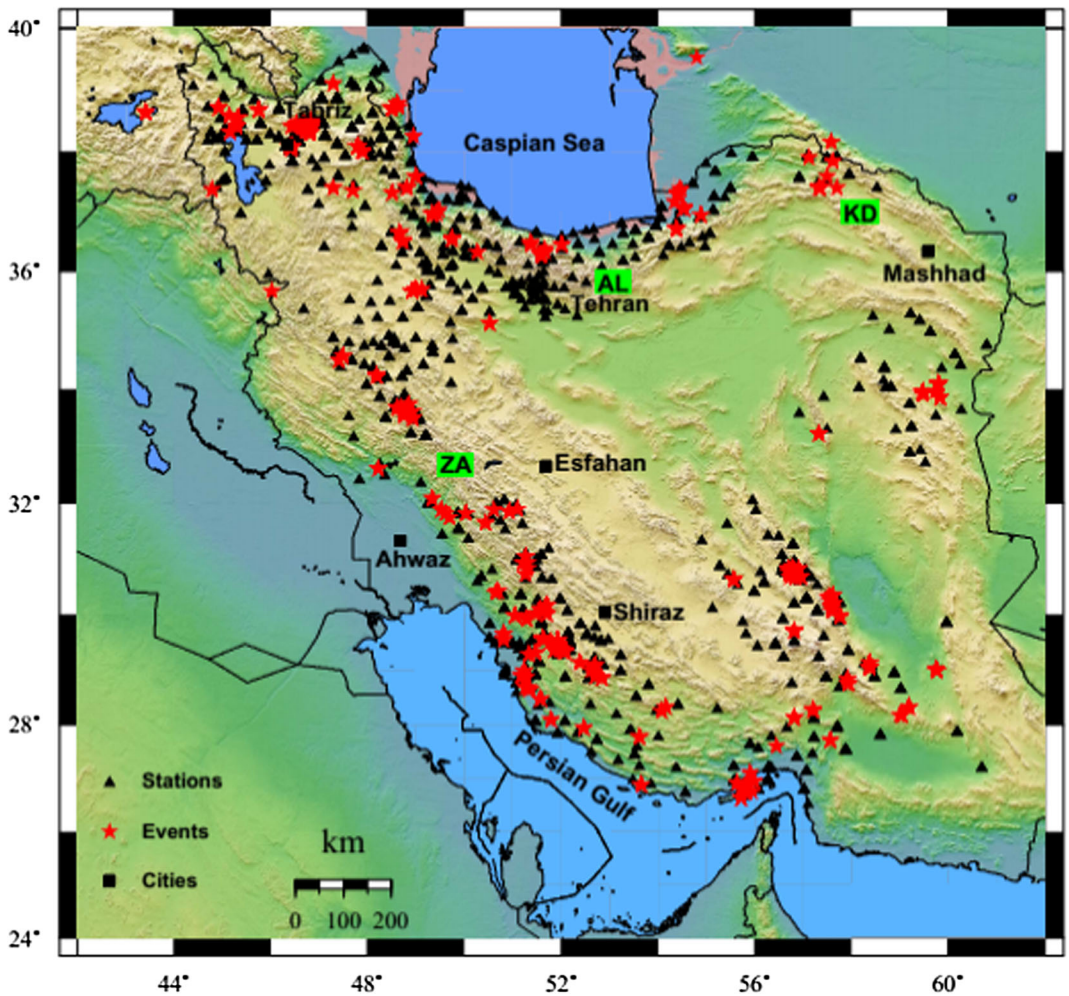

Fig. 1 Location of stations and events used in the current study. ZA marks the Zagros, AL the Alborz, and KD the Kopeh Dagh mountain range

Zafarani et al. (2008) and Zafarani and Soghrat (2012) nor Ghasemi et al. (2009a) models contain style of faulting terms. Also, Ghasemi et al. (2009a) and Saffari et al. (2012) have a simple functional form that does not include terms for the quadratic dependence of ground motions on magnitude and magnitude-dependent decay rate (e.g., Boore and Atkinson 2008).

Recently, Zafarani and Mousavi (2014), using the LH (likelihood) and LLH (log likelihood) schemes by Scherbaum et al. (2004, 2009), have shown similar performance of the Ghasemi et al.'s (2009a) empirical relations, based on the Iranian plateau database, and the Soghrat et al.'s (2012) equations, derived specifically for northern Iran. However, it should be taken into account that the applied statistical methods assess overall goodness of fit of data to a predictive model. In other words, all aspects of the model capability for prediction of strong motions are evaluated in a lumped manner and, therefore, if one of the model components is incorrect, its effect might be hidden through compensating errors in the comparison process of normalized residuals to the standard normal distribution (Scasserra et al. 2009).

Actually, due to the limited data used by Ghasemi et al. (2009a) and Saffari et al. (2012) and also strong trade-offs between different terms of GMPEs (e.g., terms corresponding to the scaling of ground motions with magnitude and geometric and anelastic decay coefficients), it is unlikely that realistic values of these terms could be obtained.

Moreover, though the local model of Ghasemi et al. (2009a) adequately fit the limited database of northern Iran, care must be taken when using this model in a seismic hazard project, especially for low probability levels. This is due to the fact that usually in PSHA applications, empirical GMPEs would be extrapolated beyond their range of validity, which may result in unexpected and undesirable results (Musson 2009). This is especially critical for local empirical models with simple functional forms as is the case for Ghasemi et al. (2009a) and Saffari et al. (2012).

This illustrates the need to update local models and to develop more elaborate functional forms of GMPEs (see Akkar and Cagnan (2010) for a similar case in Turkey). The richer database of the current study allows improving on prior works by considering additional variables that could not previously be adequately constrained.

Here, taking into account the criteria suggested by Cotton et al. (2006) and Bommer et al. (2010) such as covering an adequate range of magnitude and distance in the database, usable period range for response spectral ordinates in developed models and regression method to consider intra and inter-event error, a functional form similar to Boore and Atkinson (2008) has been used to derive local empirical GMPEs for PGA, and spectral accelerations up to period of 4 s for Iran. The Boore and Atkinson (2008) model, applied to other regions such as Italy and Turkey (e.g., Bindi et al. 2014), includes magnitude saturation and magnitude-dependent decay with distance. The selection of functional form was also supported by inspection of residual plots as will be discussed in the following sections. However, it should be noted that Boore and Atkinson (2008) implemented the simplest functional form among NGA (next generation attenuation) equations (Power et al. 2008), which does not include factors such as depth-to-top of rupture, hanging wall/footwall terms, or basin effect.

Finally, it should be noted that taking into account the empirical base of GMPEs developed in the current study will not suppress the use of simulation-based equations of Zafarani et al. (2008), Soghrat et al. (2012), and Zafarani and Soghrat (2012). The new local equations could be used along with these simulation-based GMPEs through a logic tree framework (Budnitz et al. 1997) in order to capture epistemic uncertainty.

2 Dataset

The Iranian plateau, located between the Arabian and Eurasian plates and characterized by shallow crustal faulting, can be classified as one of the most active tectonic regions in the world. The active deformation of Iran is mainly controlled by the Arabian–Eurasian plate convergence. The effect of the Arabia–Eurasia collision is accommodated by distributed faulting in the Zagros, to the south, and the Alborz and Kopeh Dagh, to the north (Fig. 1). The understanding of the active shortening in Iran is rapidly improving due to repeated GPS measurements and recent geological and paleoseismological investigations (e.g., Khodaverdian et al. 2015). From the seismotectonic point of view, different authors have classified several provinces for Iran (e.g., Takin 1972; Nowroozi 1976; Berberian 1976 and Mirzaei et al. 1998). However, in a broad framework, and for the purpose of development of empirical GMPEs, all parts of Iran can be treated as one unit (see

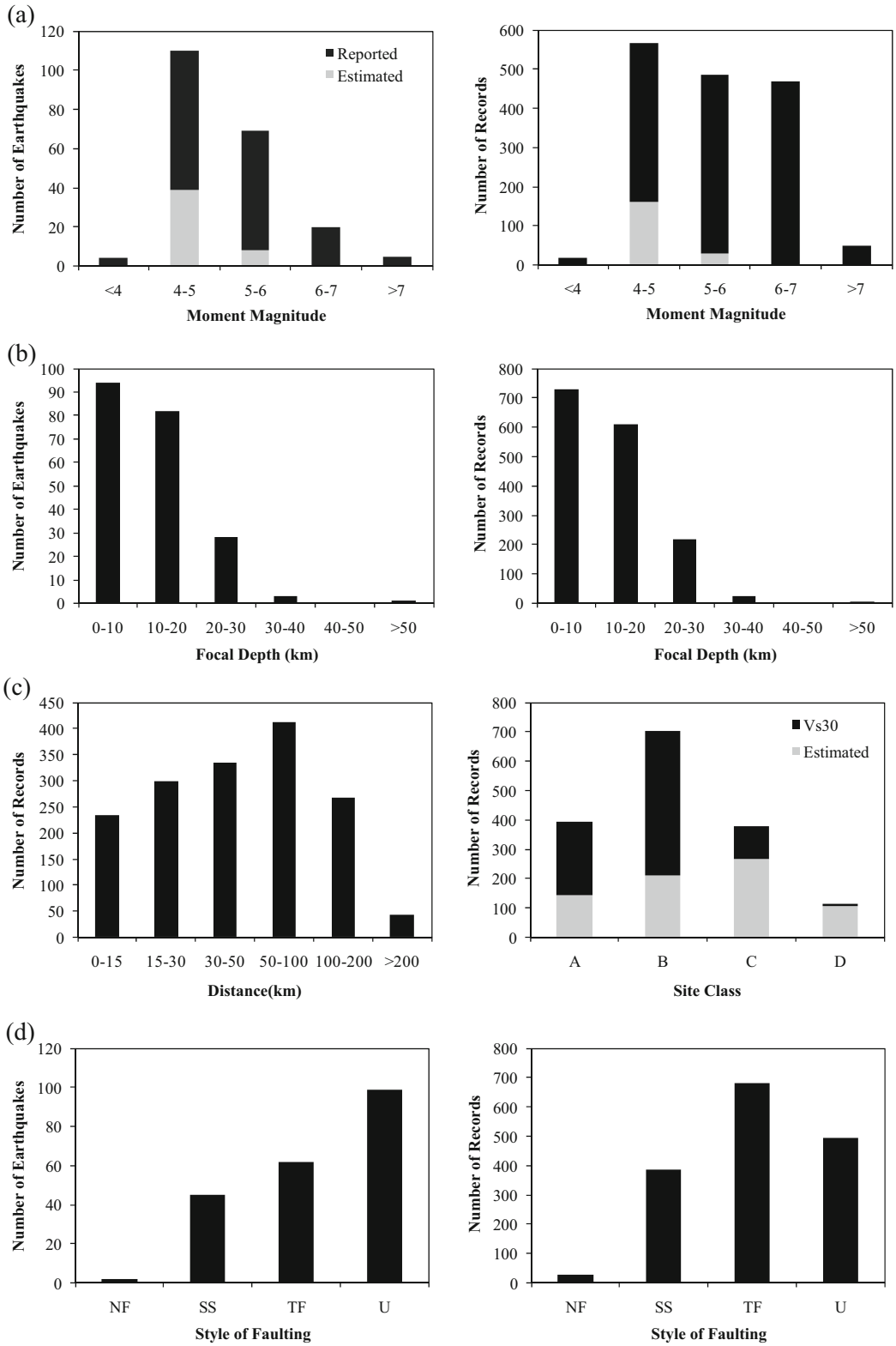
(a)
Number of Earthquakes
Reported
Estimated
<4
4-5
5-6
6-7
>7
Moment Magnitude
Number of Records
Moment Magnitude
(b)
Number of Earthquakes
0-10
10-20
20-30
30-40
40-50
>50
Focal Depth (km)
Number of Records
Focal Depth (km)
(c)
Number of Records
0-15
15-30
30-50
50-100
100-200
>200
Distance(km)
Vs30
Estimated
A
B
C
D
Site Class
(d)
Number of Earthquakes
NF
SS
TF
U
Style of Faulting
Number of Records
Style of Faulting

◀ **Fig. 2** Histogram of high-quality recorded earthquakes from strong-motion database of Zafarani and Soghrat (2017a) in terms of **a** magnitude, **b** depth, **c** distance, site class, and **d** style-of-faulting (the means of NF, SS, TF and U are normal, strike-slip, thrust and unknown faulting). Left and right columns in **a**,**b**, and **d** show the number of earthquakes and records, respectively

Zafarani and Soghrat 2012; Zafarani and Mousavi 2014 for more details). Some authors (e.g., Zafarani et al. 2008; Ghasemi et al. 2009a; Kale et al. 2015) have derived GMPEs for the Iranian plateau as a whole.

In Iran, strong-motion recording history goes back to the early 1970s. Data are recorded by the Iranian Strong Motion Network (ISMN), operated by the Building and Housing Research Center (BHRC), consisting of more than 1100 three-component accelerograph stations (most of which are equipped with Kinemetrics SSA-2 digital accelerographs). The early efforts to investigate strong motion characteristics of Iran and to develop local GMPEs, based on the limited observations, date back to the large and catastrophic earthquakes of 16 September 1978 (Tabas, M_w 7.4; Shoja-Taheri and Anderson 1988) and 21 June 1990 (Rudbar-Manjil, M_w 7.3; Berberian et al. 1992). Since then, the ISMN collection has gradually expanded to about 10,000 records, archived by the end of 2013. Recently, Zafarani and Soghrat (2017a) have compiled a comprehensive, high-quality strong-motion dataset which contains data from earthquakes recorded by at least two stations. A careful revision of the characteristics of the earthquakes such as location, magnitude, style of faulting, and fault rupture plane geometry has been performed for the first time using the best available information in a scientifically sound manner. About 1500 shear wave velocity profiles derived by seismic refraction tests performed by BHRC have been collected to characterize the site condition of the Iranian accelerometric stations.

The database for regression is a subset of this recently compiled database of strong motions from Iranian earthquakes (Zafarani and Soghrat 2017a). For further details about the description of the database and procedures for the determination of event magnitude, style of faulting, selection and calculation of distance measure, and site condition, the reader shall refer to Zafarani and Soghrat (2017a). The early version of the database has been already used in a number of previous strong-motion studies in the Iranian plateau (Zafarani and coworkers, 2007–2014); however, a major expansion and upgrade has been completed recently that increased the number of records to more than 10,000 three-component records. The compilation consisted of merging, expanding, and upgrading the local databases provided by Zafarani and coworkers for the Zagros (Zafarani et. al. 2012; Zafarani and Soghrat 2012; Zafarani and Hassani 2013), northern Iran (Soghrat et al. 2012), and east-central Iran (Zafarani et al. 2008). We also added

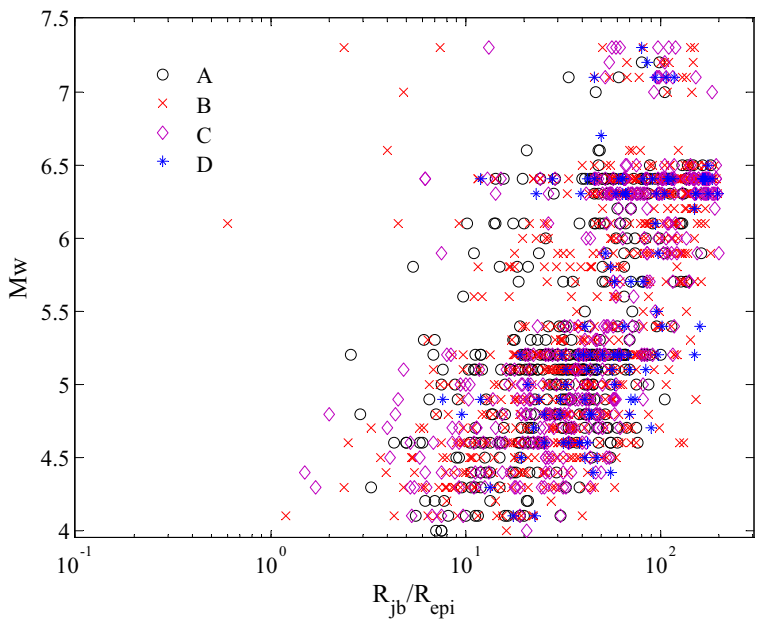

Fig. 3 Magnitude-distance distribution of the employed ground motion records, EC8 site classes are also shown. R_{JB}/Repi means R_{JB} or Repi

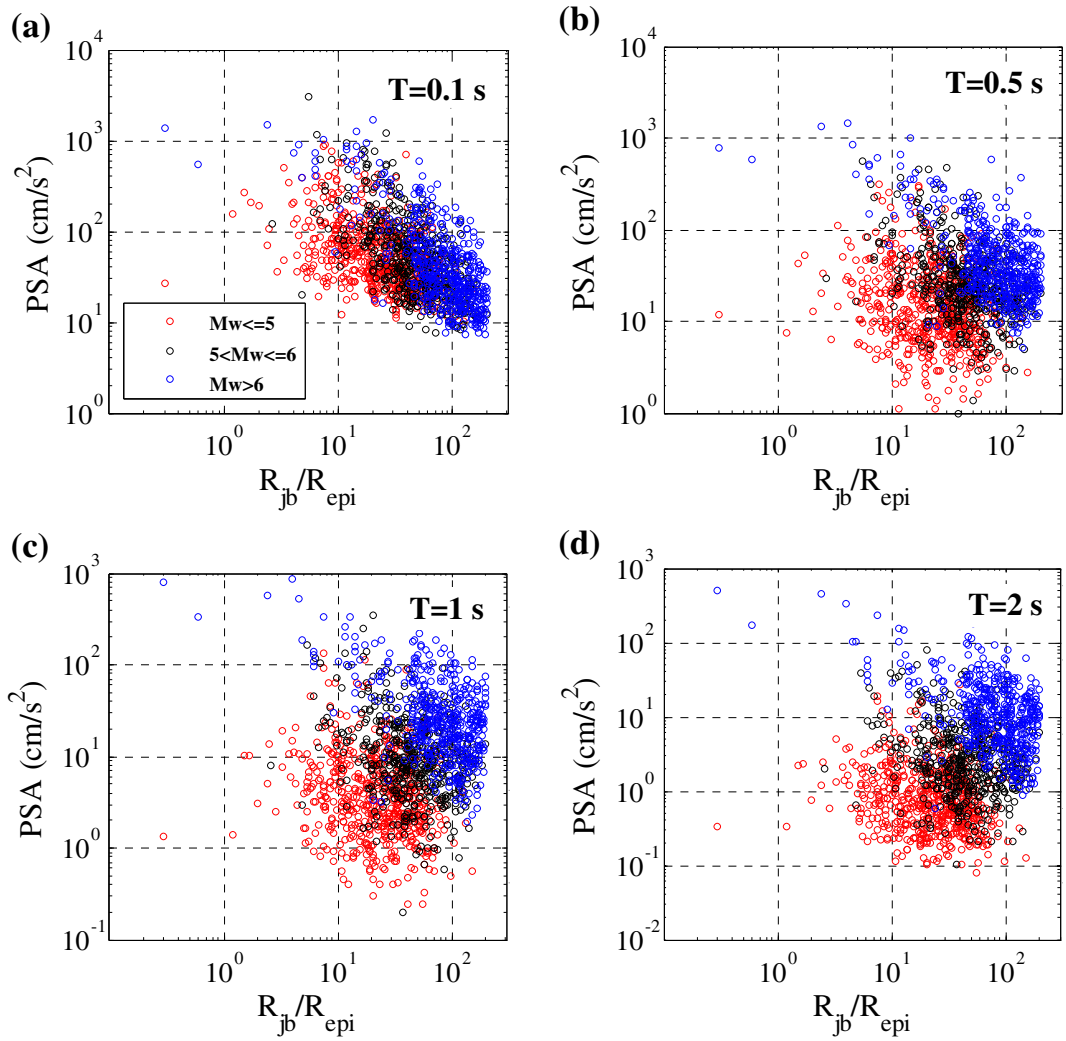

Fig. 4 Distribution of PSAs versus distance at (**a**) PGA and periods of (**b**) 0.5, (**c**) 1 and (**d**) 2 s

data from recent Iranian earthquakes (2010–2014). The earthquake metadata are compiled from reliable national and international seismological agencies to obtain source geometry and distance parameters for each event. Moment magnitudes are obtained from the international seismological agencies or other published resources or converted from other magnitude scales using the empirical relations of Shahvar et al. (2013). Focal mechanisms and depths were also obtained from national and international seismological agencies. The bulk of the mechanisms of events are reverse and strike-slip, while normal faulting is rare, contrary, e.g., to the Italian dataset. It means that in the database for about 66% of the events, there is no available information about their faulting mechanisms. The dominant faulting mechanisms in the remaining are reverse (20% of the events) and strike-slip faulting (12% of the events). Only 1% of events are related to normal faulting mechanism (for more details, it can be referred to Zafarani and Soghrat 2017a).

Horizontal distances to the surface projection of the rupture plane (i.e., the Joyner–Boore distance, R_{JB}) have been calculated for large earthquakes (M > 6.0). When available, sites have been classified on the basis of the average shear wave velocity to a depth of 30 m (Vs30) and each station was assigned an EC8 site class. In the absence of shear wave profiles, site classification was based on the empirical methods of Zare et al. (1999) and

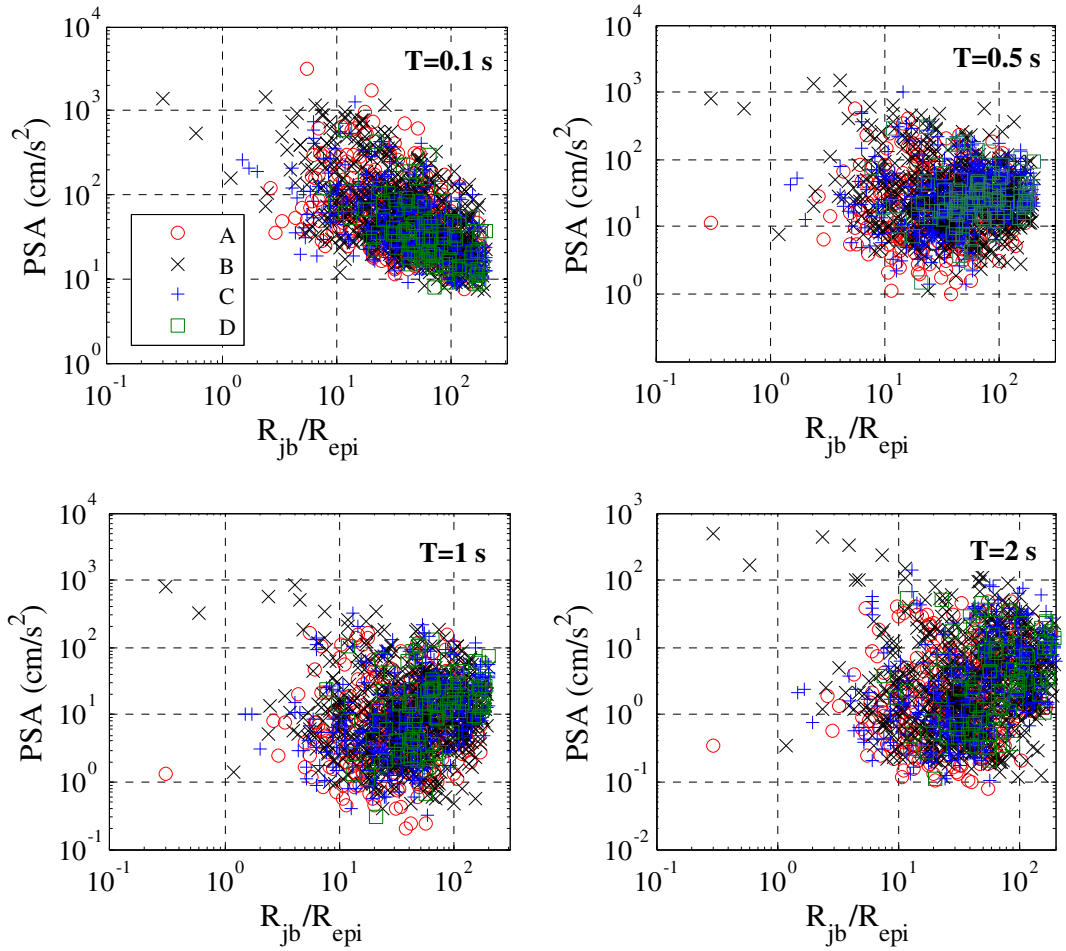

Fig. 5 Distribution of PSAs versus distance for different site conditions

Ghasemi et al. (2009b). Figure 2 shows the histograms of a subset of the database containing data from earthquakes with at least two high-quality free-field records with known site condition. The histograms are plotted with respect to magnitude, depth, site class, and focal mechanism. It should be mentioned that the means of "Reported" in the figure is the moment magnitude which is provided from international or local seismological agencies or from earthquake-specific literature studies. Moreover, wherever the moment magnitude is not available, the empirical magnitude conversion equations of Shahvar et al. (2013) have been used to obtain the more homogenous magnitude information which is called "Estimated."

Taking into account the scarcity of data from earthquakes with $M_w < 4.0$, and records with distance larger than 200 km, and their minor significance for PSHA studies in Iran, they have been excluded from the regression analysis. In addition, data from few earthquakes with normal faulting mechanism and earthquakes at depths > 30 km are discarded.

To develop the empirical GMPEs, we used 1551 three-component free-field records from 200 earthquakes with $M \geq 4.0$ and distance < 200 km, having at least two high-quality records and known site condition. The uncorrected acceleration time series recorded by a given station were corrected for the instrument response and baseline, following a standard algorithm (Trifunac and Lee 1973). Multi-resolution wavelet analysis (Ansari et al. 2010) was performed to remove undesirable noise from the recorded signals. Figure 3 shows the magnitude–distance distribution of the employed ground motion records, differentiated by site type. Iranian data are scarce for $M < 5.5$ and $R_{JB} > 100$ km and

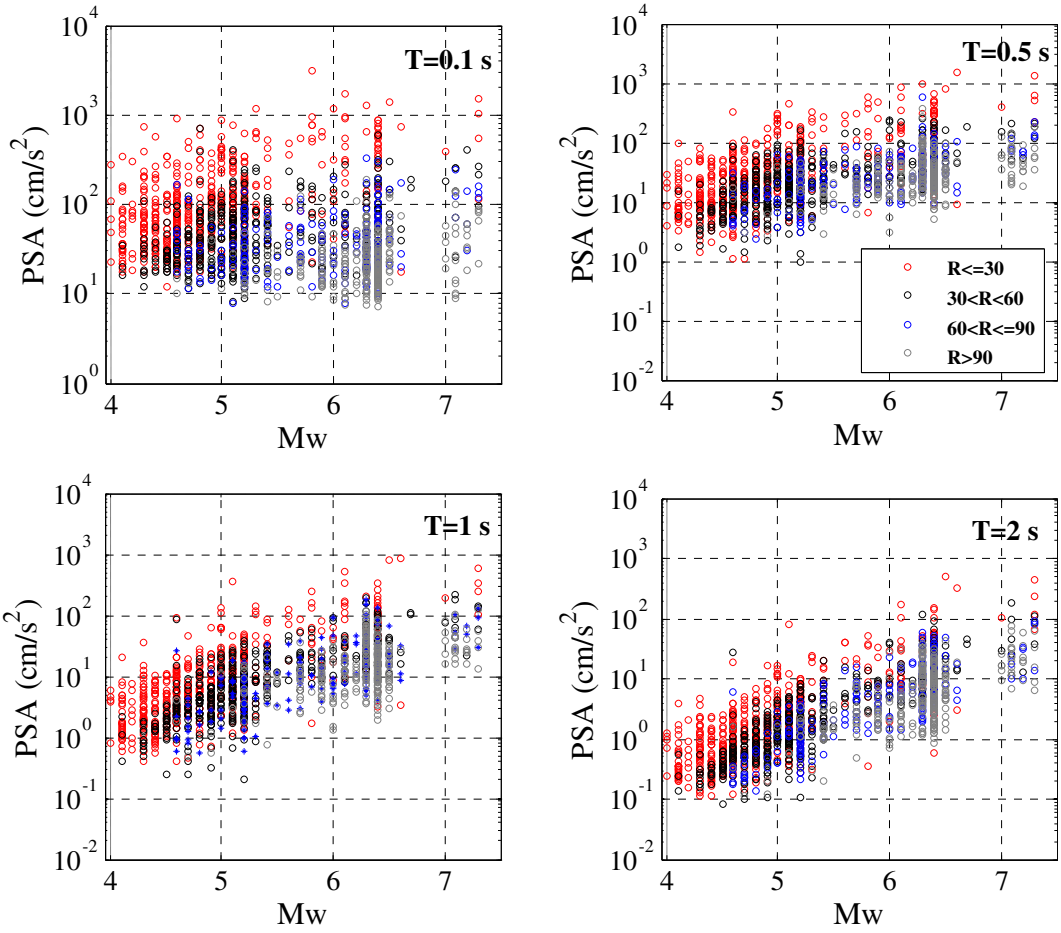

Fig. 6 Distribution of PSAs versus moment magnitude

this implies that ground motions for small events at large distances will not be sufficiently constrained by observations. Moreover, the data set contains 13 events with magnitude larger than 6.5, 7 of which having magnitude larger than 7. However, these larger events usually have lack of recording at close distances. Figures 4, 5, and 6 show, respectively, the distance and magnitude dependence of 5%-damped PSA at four periods (T = 0.1, 0.5, 1, 2 s). These figures show the distribution of data in terms of spectral ordinates and distance. It shows that the regression results can be reliable in the wide range of distance and magnitude considering different site classes.

Although different horizontal component definitions have been used in the literature, we decided to adopt the geometric mean of horizontal components, taking into account that some studies have shown that the ratio of this measure over the rotation-independent average horizontal component (GMRotI50), used in the NGA models, is near unity at all periods (Beyer and Bommer 2006).

An explorative analysis has been conducted by calculating the total residuals using the Pan-European GMPEs of Akkar and Bommer (2010) and Bindi et al. (2014), which include Iranian data. Figure 7 shows the total residuals (i.e., the subtraction of logarithms of observed and predicted spectral amplitudes) plotted against distance (epicentral or Joyner-Boore distance). Both GMPEs seem inadequate to represent short period ground motions (0.1 s and 0.3 s), as the residuals of Bindi et al. (2014) are generally positive, at distances larger than 10 km, indicating an under-prediction of observations and the residuals of Akkar and Bommer (2010) exhibit a bump at intermediate distances. On the other hand, ground motions at long periods seem better represented than the short periods. This lack of fit could

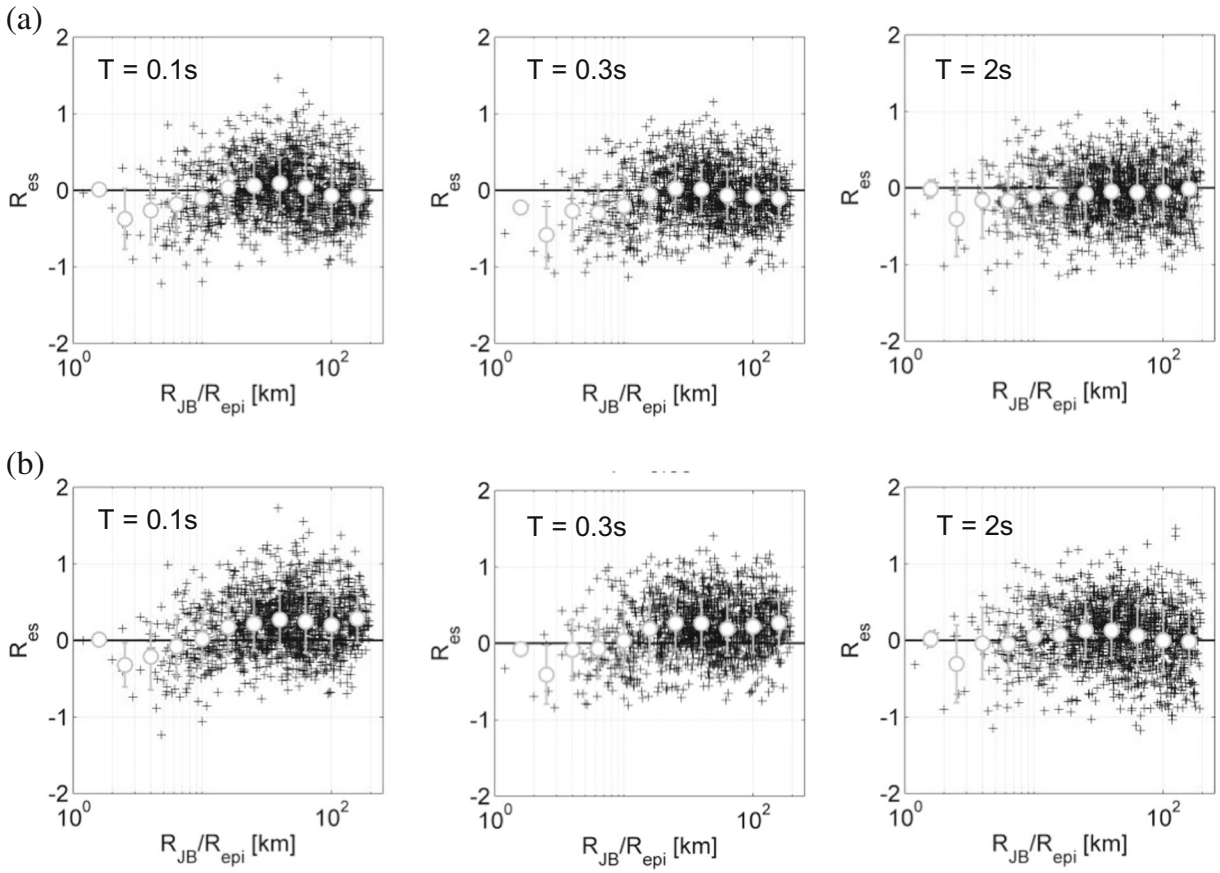

Fig. 7 Residuals calculated using **a** AB10; Akkar et al. (2010) and **b** BND14; Bindi et al. (2014). R_{JB} /Repi means R_{JB} or Repi. The residual shows the differences between predicted and observed values

suggest that GMPEs derived from a broad data set (e.g., regional data set of pan-European or Europe and the Middle East) could not capture local features, as in the case of Iran. Therefore, the availability of a large amount of records, specific of this region, is an opportunity to derive a set of equations that can better represent the mean expected ground-motion parameters and the associated variability.

3 Regression analysis

The equation employed for the regression was initially proposed by Boore and Atkinson (2008). Afterwards, Bindi et al. (2011) used this functional form, neglecting the nonlinear site terms and accounting for a different site classification. After trying different functional forms, and comparison between the observed and predicted values as well as the available biases, the following equation was finally used in this study:

$$\log_{10} Y = e_1 + F_D(R, M) + F_M(M) + F_S + F_{\text{sof}} + \varepsilon\sigma \quad (1)$$

where Y represents the strong-motion parameters; e_1 is a constant term; F_{D}(R, M), F_{M} (M), F_{S}, and F_{sof} represent the distance function, the magnitude scaling, the site amplification, and the style of faulting correction, respectively. M is the moment magnitude, R is the Joyner–Boore distance, or the epicentral distance (in km), when the fault geometry is unknown. The variability is represented by the total standard deviation σ.

The magnitude function F_{M} is

$$F_M(M) = \begin{cases} b_1(M - M_h) + b_2(M - M_h)^2 & \text{for } \text{M} \le \text{M}_h \\ b_3(M - M_h) & \text{for } \text{M} > \text{M}_h \end{cases} \quad (2)$$

where M_{h} is a hinge magnitude that has been considered variable in the range 5.0–7.2, selected as a function of period (Fig. 5). The term F_{S} in Eq. (1) represents the site

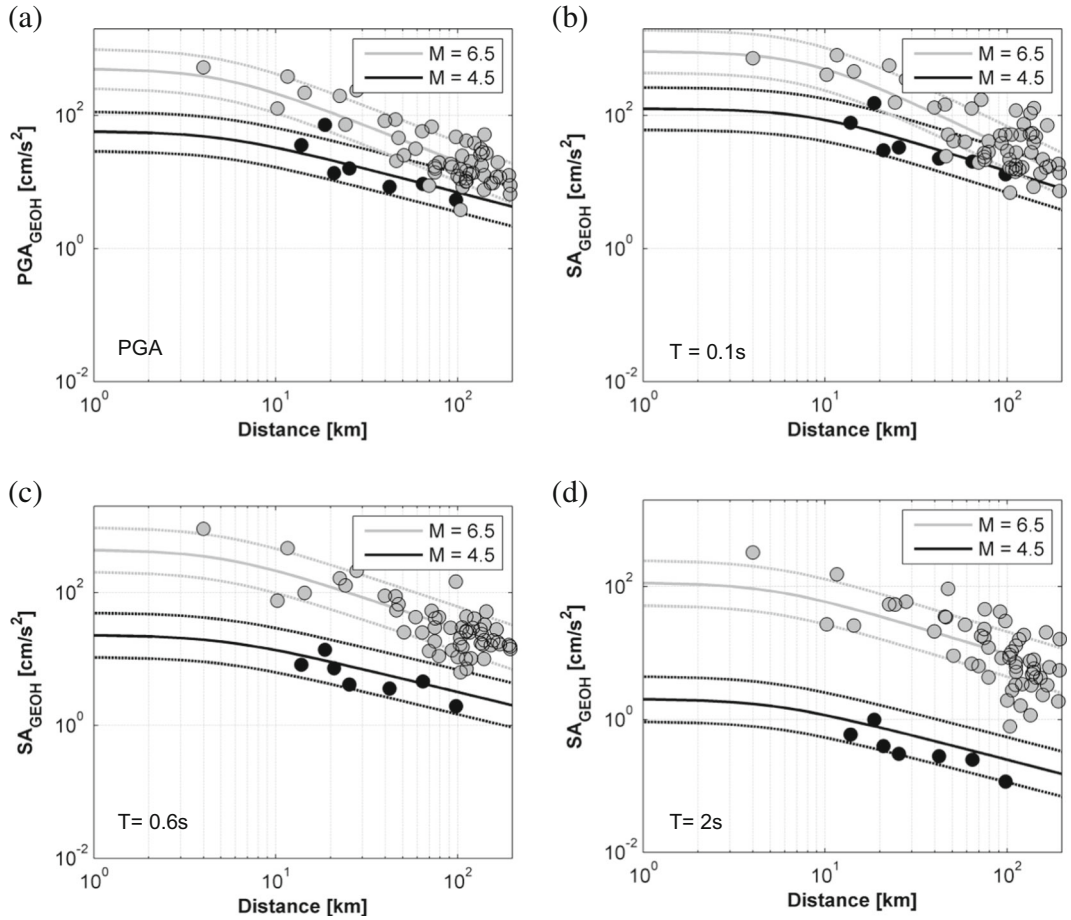

Fig. 8 Comparison between preliminary median predictions of pseudo spectral acceleration and observations at low (M4.5 ± 0.3) and moderate magnitudes (M6.5 ± 0.3) at (**a**) PGA and periods of (**b**) 0.1, (**c**) 0.6 and (**d**) 2s. The curves have been calculated for strike-slip mechanism and site class B

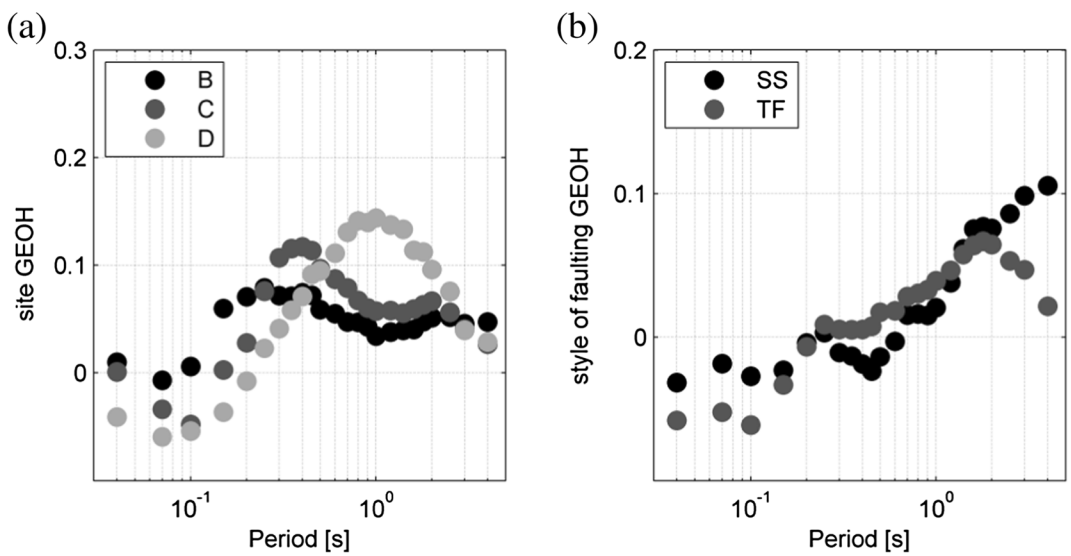

Fig. 9 Coefficients of site classes (left column) and style of faulting (right column) versus period

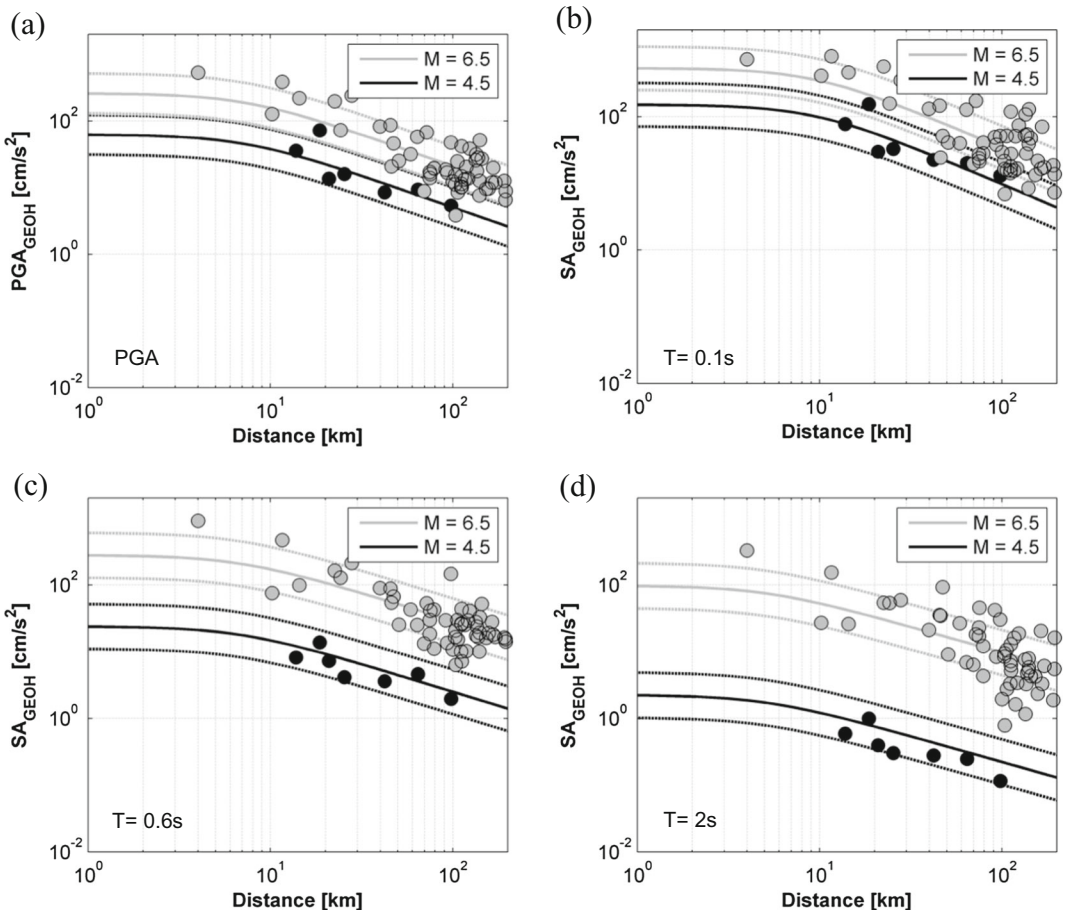

Fig. 10 Comparison between median predictions of pseudo spectral acceleration and observations at low (M4.5 ± 0.3) and moderate magnitudes (M6.5 ± 0.3) at (**a**) PGA and periods of (**b**) 0.1, (**c**) 0.6 and (**d**) 2s, for a strike-slip fault and site class B

amplification given by $F_S = s_j\, C_j$, for $j = 1,...,4$, where s_j are the coefficients to be determined through the regression analysis and C_j are dummy variables used to denote the four different EC8 (Eurocode 8) site classes (A, B, C, and D according to EN-1998-1: 2003). The functional form F_{sof} represents the style of faulting correction given by $F_{sof} = f_j E_j$, for $j = 1,...,3$, where f_j are the coefficients to be determined during the analysis and E_j are dummy variables used to denote the different fault classes. We considered three style of faulting in the analysis: thrust (TF), strike slip (SS), and undefined (U). The regressions were performed setting to zero for the EC8 site class A (as a reference site class) as well as the undefined style of faulting.

The anelastic attenuation term is usually included to accommodate extrapolation of the models beyond the 200 km limit of the dataset, which is sometimes unavoidable in probabilistic seismic hazard analysis. Also, the four NGA-West2 GMPEs (Gregor et al. 2014) provide regional versions through region-dependent anelastic attenuation term (for Japan, Italy, Turkey and Taiwan). However, in almost all previous regional models for Europe, the Mediterranean region, and the Middle East (e.g., Ambreraseys et al. 2005, Bindi et al. 2014), the coefficients on this term were found to be positive, which is not acceptable as it hints an increase in amplitudes of ground motions with increasing distance, so none of the final regional models include this effect. Therefore, it has not been considered in the current regression analysis, as well.

The geometrical spreading term is similar to Bindi et al. (2011):

$$F_D(R,M) = [c_1 + c_2(M - M_{ref})]\log_{10}\left(\frac{\sqrt{R_{JB}^2 + h^2}}{R_{ref}}\right) \quad (3)$$

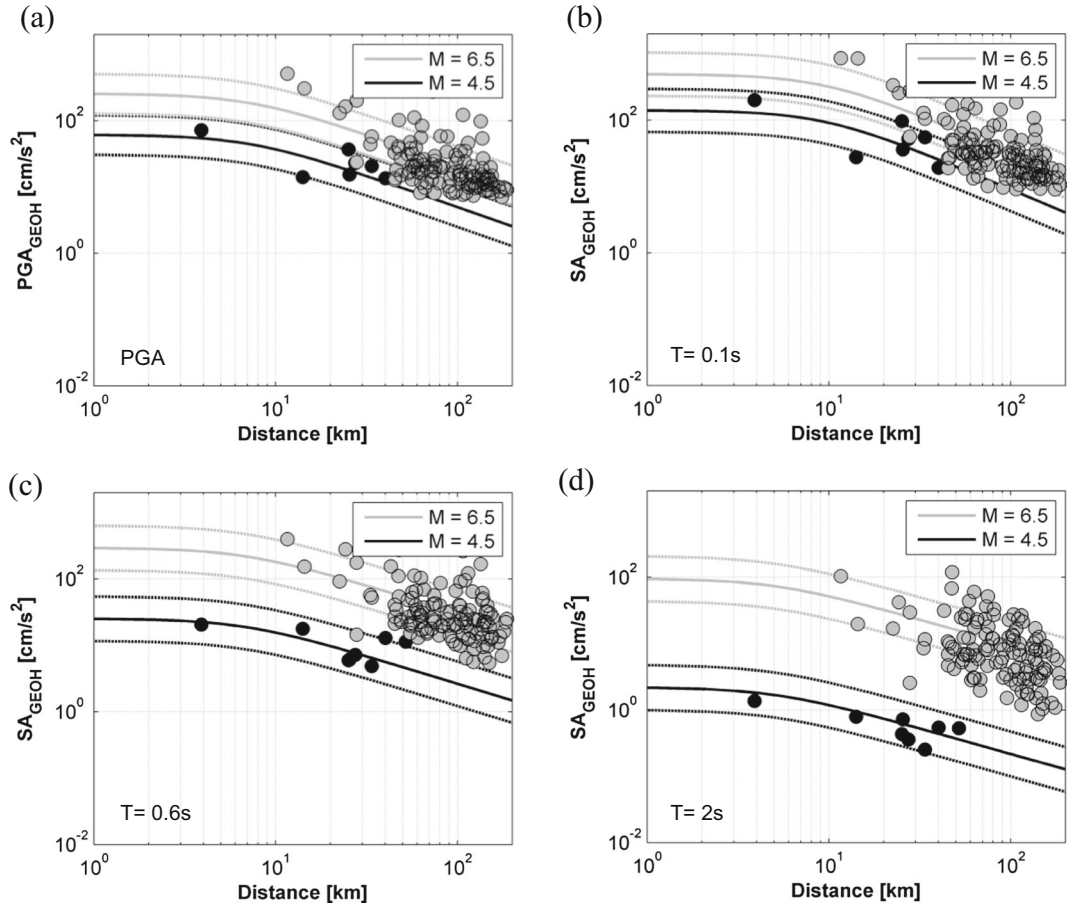

Fig. 11 Comparison between median predictions of pseudo spectral acceleration and observations at low (M4.5 ± 0.3) and moderate magnitudes (M6.5 ± 0.3) at (**a**) PGA and periods of (**b**) 0.1, (**c**) 0.6 and (**d**) 2s, for a thrust fault and site class B

where M_{ref} denotes the reference magnitude, R_{ref} is the reference distance, and h is a pseudo-depth, to be determined through the regression analysis. According to the Boore and Atkinson (2008) "the pseudo-depth h in the regression is used to avoid overlap in the curves for large earthquakes at very close distances". The value of R_{ref} is fixed to 1 km at all periods after some trial regressions (similar to Boore et al. 2014 and Bindi et al. 2014). This equation includes a magnitude-dependent geometric attenuation through the coefficient c_2. Preliminary results gave negative c_2 coefficients, indicating that ground motion associated to smaller magnitude events with $M < M_{ref}$ attenuate less than large ones at periods less than 1.0 s (Fig. 8).

We believe that the scarcity of data from small earthquakes ($M < 5$) at large distances is the cause of such unrealistic behavior. Kale et al. (2015) have also pointed out the scarcity of Iranian data for $M < 5.0$ and $R_{JB} > 80$ km and computed the magnitude-dependent regression coefficients only for distances up to 80 km.

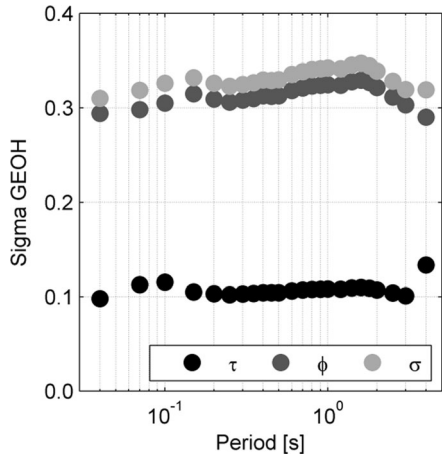

Fig. 12 Period-dependent total (σ), between-event (τ), and within-event (ϕ) standard deviation

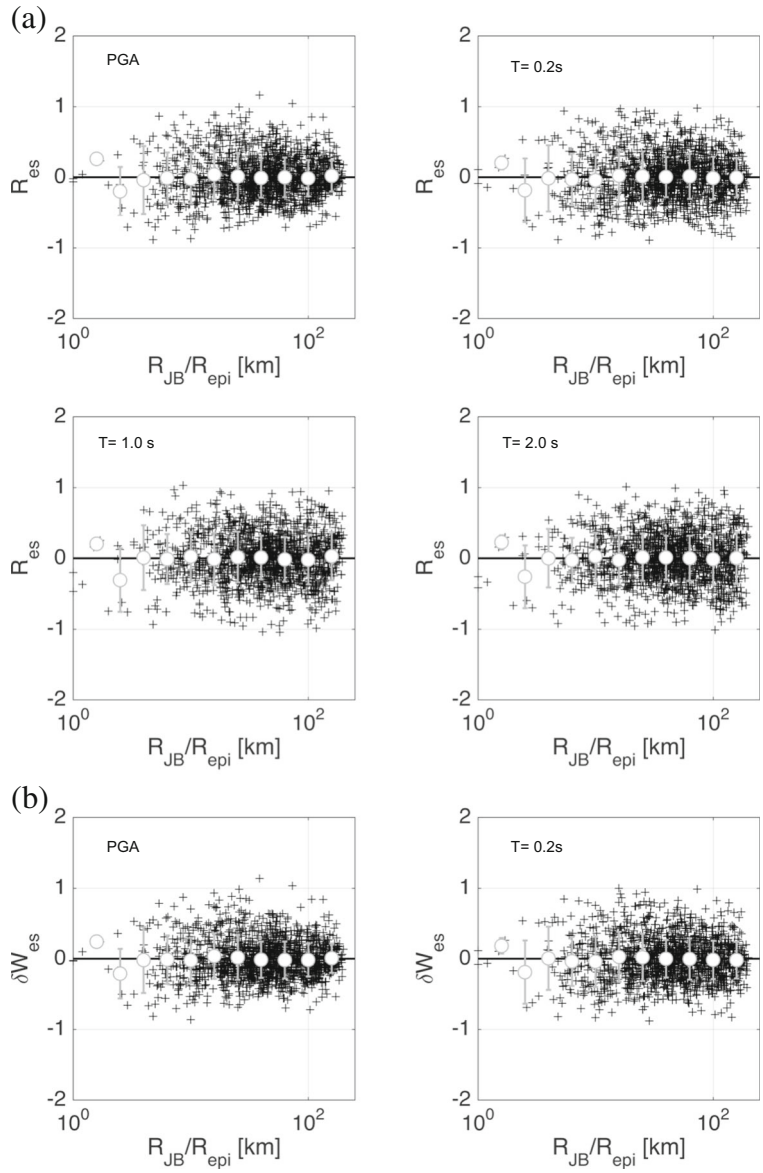

Fig. 13 Residuals distributions at four selected periods (PGA, 0.2, 1 and 2 s); **a** total residuals Res versus distance; **b** within-event residuals δWes versus distance and **c** between-event residuals δBe versus magnitude

As a final assumption, the coefficient for magnitude-dependent attenuation c_2 is set to be null, as insufficiency of data precluded the investigation of the geometric decay rate of small earthquakes beyond ~ 100 km.

The regression has been performed by applying a random effect approach (Abrahamson and Youngs 1992). The residuals δR_{es} have been calculated as the logarithmic difference between observations and predictions; then, the components of the variability have been separated as (Al Atik et al. 2010):

$$\delta R_{es} = \delta B_e + \delta W_{es} \tag{4}$$

where the subscript e is referred to the events and the subscript s to the stations. δB_e is the between-events residual, calculated as follows:

$$\delta B_e = \frac{1}{NS} \sum_{s=1}^{NS} \delta R_{es} \tag{5}$$

and δW_{es} is within-event residual, which is the difference between total and between-event residuals. The within-

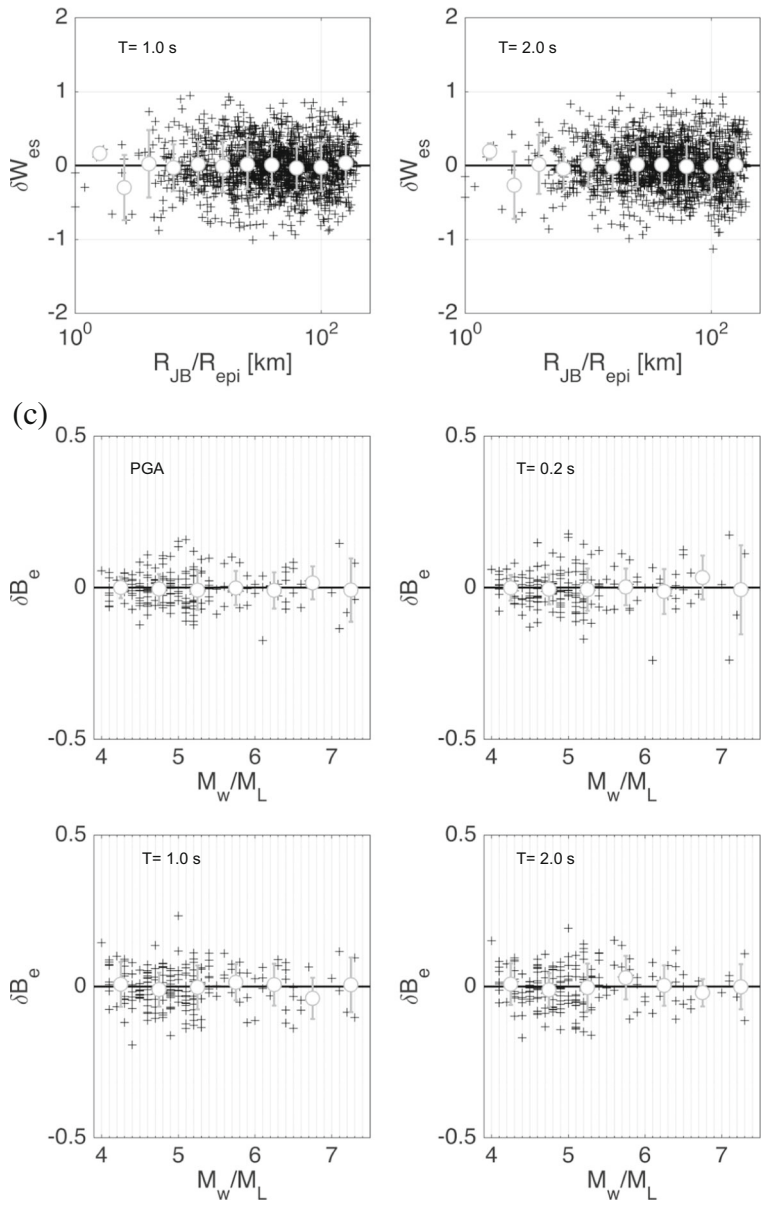

Fig. 13 (continued)

event residuals show the difference between the observed and the median ground motion at a distance for a particular event while the between-event residuals indicate the difference between the average level of ground motion for an event and the expected level for that event.

The parameters considered for the regressions are the peak ground acceleration (PGA, in cm/s^2) and the 5%-damped acceleration response spectra (PSA, cm/s^2) in the period range 0.04–4.0 s.

The prediction equations have been provided both for the geometrical mean of the horizontal components (hereinafter GEOH) and the vertical-to-horizontal ratio (V/H). After evaluation of seismic hazard in the framework of probabilistic approach for horizontal component, the response spectra of vertical components can be retrieved by scaling horizontal spectra with appropriate V/H spectral ratios (Bommer et al. 2011).

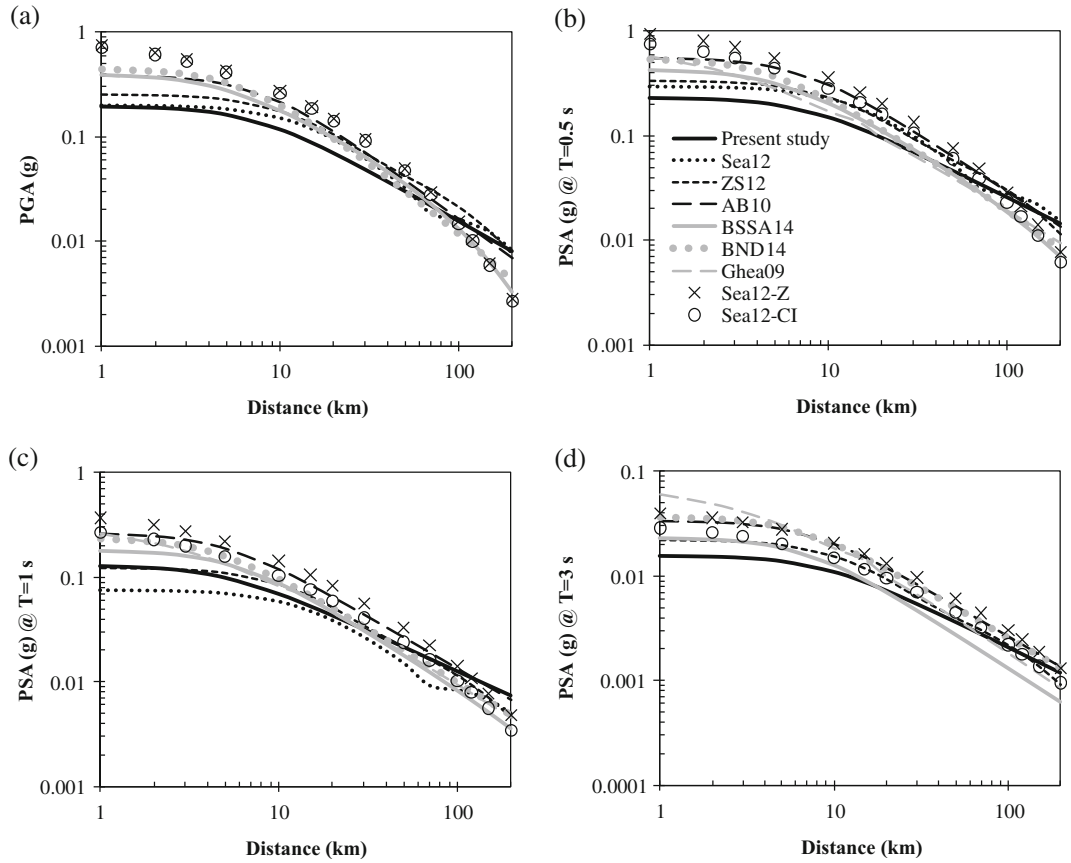

Fig. 14 Comparison of PSA of proposed model with some global, regional and local models, For Mw=6.0, site class B and thrust faulting at (**a**) PGA and periods of (**b**) 0.5, (**c**) 1 and (**d**) 3 s. Sea12: Soghrat et al. (2012), ZS12: Zafarani and Soghrat (2012), AB10: Akkar and Bommer (2010), BSSA14: Boore et al. (2014), BND14: Bindi et al. (2014), Ghea09: Ghasemi et al. (2009a), Sea12-Z: Saffari et al. (2012) for Zagros region and Sea12-CI: Saffari et al. (2012) for Central Iran

4 Results

The regression coefficients, the hinge magnitude M_h, and the standard deviation components obtained for GEOH and V/H ratio are given in Appendix (Tables 1 and 2). Figure 9 shows the site class and focal mechanism coefficients obtained from the regression for GEOH.

The results for the site coefficients evidence similar site effects of classes B and C, although at low periods (< 0.15 s), the coefficient of class B is close to the reference site, while classes C and D show slightly de-amplification. At intermediate to long periods, the coefficients are always positive: class D shows the highest value (about 0.15) at 1 s, while the maximum values for classes B (0.08) and C (0.11) are reached in the period range 0.3–0.4 s. Negative values of coefficients SC and SD at short periods ($T < 0.2$ s) means these site classes, although having smaller Vs30 (softer soil), de-amplify the motions with respect to site class A. Recently, using the square-root-impedance method to estimate site amplification in Iran, it has been shown that although the softer classes in the Iranian plateau (the ones with lower Vs30) have higher amplifications at lower frequencies, the trend is completely reversed at higher ones (Jahanandish et al. 2017). Frequencies at which the peaks of coefficients occur are different from previous studies for other regions. In Akkar and Bommer (2010), stiff and soft sites have the maximum amplitude at about 1.3 s while in Bindi et al. (2014) class B, C, and D sites have peaks at 1 s. However, Ghasemi et al. (2009b) has reported same trends as the current study, from response spectral ratio (H/V) of Iranian strong motion data. Our results are also consistent with Zare et al. (1999), who emphasized the difference between geological and meteorological conditions in Iran (i.e., a mountainous

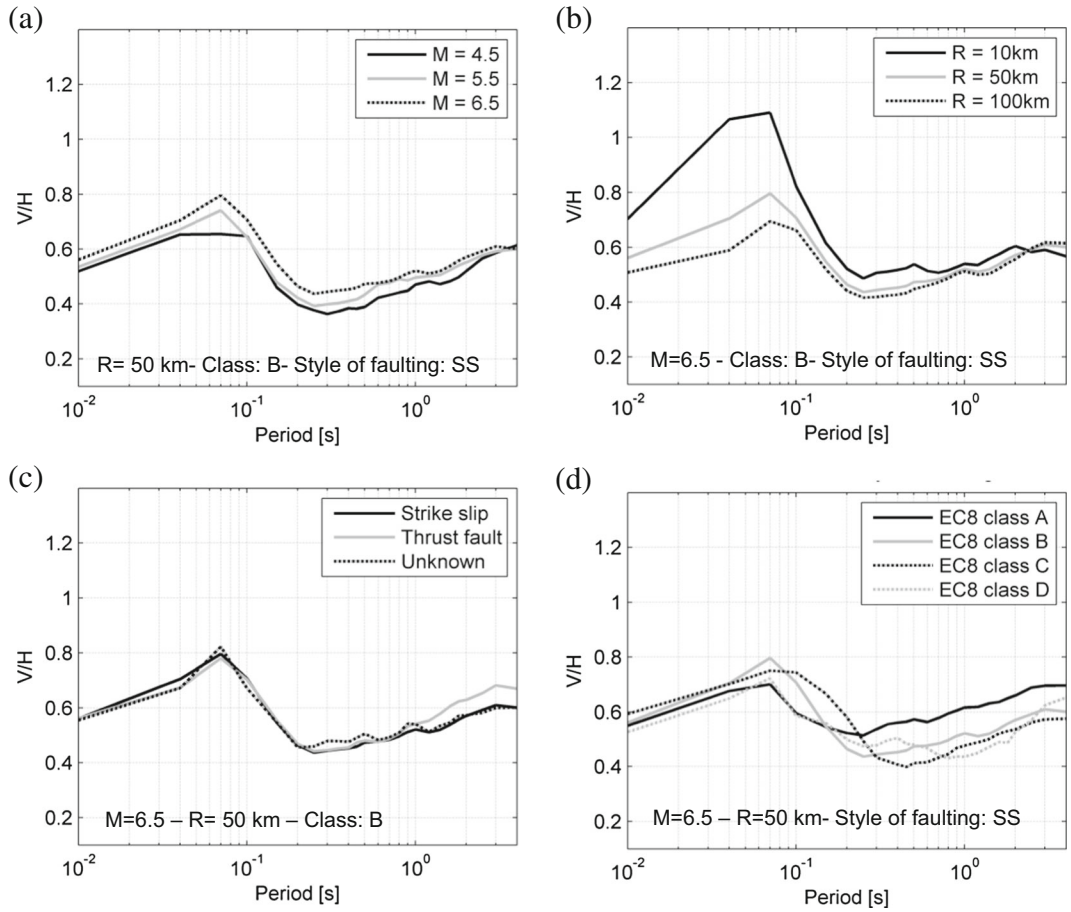

Fig. 15 Vertical-to-horizontal ratios as a function of period, showing the effect of **a** magnitude (M4.5, 5.5, 6.5), **b** distance (10, 50, and 100 km), **c** style of faulting, and **d** EC8 site class. Unless otherwise noted, V/H is evaluated for $M = 6.5$, $R = 50$ km, strike-slip mechanism, and site class B. The value of V/H at 0.01 s corresponds to PGA

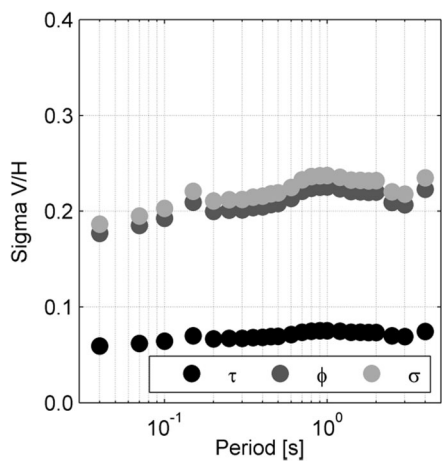

Fig. 16 Period-dependent total (σ), between–event (τ), and within–event (ϕ) standard deviations observed for the V/H ratios

country with dry weather conditions and a low water table in most areas) and other seismic areas in the Mediterranean region such as Italy and Turkey. Moreover, they concluded that there are a small number of sites with low frequency amplification in contrast with the many sites with moderate amplifications in the intermediate and high frequency range.

On the other hand, the styles of faulting coefficients follow a similar trend as Bindi et al. (2014), as shown in Fig. 8.

In Figs. 10 and 11, the median prediction for the PSA ordinates (PGA, periods 0.1, 0.6, and 2 s) over distance is compared to observations for EC8 B sites (best sampled sites), for magnitudes 4.5 and 6.5. Two focal mechanisms are considered: Fig. 10 represents strike slip events, while Fig. 11 thrust fault events.

Figure 12 shows the total (σ), between-event (τ), and within-event (ϕ) standard deviations as a function of period. The total variability σ of the model gradually increases with period, from 0.31 (log10 units) at 0.04 s, up to 0.35 at 1.6 s. The between-event variability τ is quite low and equals about 0.1, over the entire period range (0.04–4.0 s). As a result, the within-event standard deviation ϕ is similar to σ and is less influenced by sigma decomposition. The difference between the two standard deviations (ϕ and σ) is about 5.5% if averaged over the entire period range. The between-event error depends on the quality of event metadata (location, magnitude, etc.); therefore, low between-event error means a good-quality dataset and a reduction of the epistemic uncertainty in PSHA results. However, the total standard deviations of our model are close or a bit more than the standard deviations of recent NGA-West2 models (Gregor et al. 2014).

Figure 13 shows the distribution of the total R_{es} and within-event δW_{es} residuals as a function of distance and the between-event δB_e residuals as a function of magnitude at two periods (0.1 and 2 s). Total residuals R_{es} do not show any bias or distance dependence. Between-event residuals δB_e are plotted against magnitude and, although values are quite small, they confirm the largest variability of small events compared to moderate and large magnitude earthquakes. Finally, within-event residuals δWes are plotted against distance, confirming the absence of any trend. Recently, Zafarani and Farhadi (2017) examined the efficiency of some selected ground-motion prediction equations, including the recently published GMPEs of Ghasemi et al. (2009a), Akkar et al. (2014), and Bindi et al. (2014) against small-to-moderate data (an independent dataset) recorded in the Iranian plateau. In conclusion, they reported that the model developed in the current study as a ground-motion model valid for a magnitude range as small as M4.0 is the only model that shows good consistency with the recorded data over all frequencies.

Comparison of median predictions of PGA and PSA (at $T = 0.5$, 1.0, and 2.0 s) using the model developed in this study with those from global (Boore et al. 2014), regional (Bindi et al. 2014; Akkar and Bommer 2010), and local models (Zafarani and Soghrat 2012; Soghrat et al. 2012; Ghasemi et al. 2009a and Saffari et al. 2012) is shown in Fig. 14. The calibrated model and selected GMPE-estimated medians are compared to each other over the range of distances and magnitudes. The proposed GMPEs have lower median values than other selected models at distances less than 100 km. It should be mentioned that because of using different distance metrics in the models, the comparison has been made using the conversion relations of Kaklamanos et al. (2011) to obtain the unique distance.

Different trends between pseudo-depth and period are reported in various studies. According to the study of Boore et al. (2014), there is an increasing trend between two parameters while in another study (Bindl et al. 2014), the increasing trend is not observed over the entire period range. The trend observed in this study (Appendix Table 1) seems to be similar to Bindi et al. (2014) and Akkar and Bommer (2010). It should be mentioned that this parameter is set to a fix value (period independent) in some studies such as Akkar et al. (2014). Moreover, though some authors (e.g., Bindi et al. 2014) put an additional constraint on some regression coefficients (e.g., $b_3 > 0$), however, here we prefer to find the actual trend of data and avoid such artificial (or physics-based) constraints as much as possible (see Appendix Table 1). Here, the only coefficient that was set to zero because of such constraints was c_2. However, finally, we checked that varying the magnitude from M4.0 to M7.5, while keeping all other parameters constant, the general trends of strong motions are acceptable over the entire period range of interest.

Figure 15 shows the median vertical-to-horizontal ratios as a function of period, highlighting the effect of magnitude (a), distance (b), style of faulting (c), and site class (d). Unless differently specified, V/H is calculated for $M = 6.5$, $R = 50$ km, strike-slip mechanism, and B site class that are the most represented categories of the dataset. The trend of V/H in the current study is similar to the recent study of Soghrat and Ziyaeifar (2016) for northern Iran.

V/H ratios are generally higher at large magnitudes and short periods (< 0.1), as shown in Fig. 15a. Near-source sites exhibit higher ratios, generally higher than 2/3, or higher than 1 in short distances and at short periods (0.07–0.1 s, Fig. 15b), as already demonstrated by Bozorgnia and Campbell (2004). On the other hand, small differences are observed in the V/H, depending on the style of faulting (Fig. 15c).

Small differences are also observed for the different site classes, with the exception of class A, that at periods longer than 0.3 s exhibits larger V/H ratios, as observed in literature (Bommer et al. 2011).

The variability of V/H models is lower than the variability observed for other ground motion parameters, as already found by Bommer et al. (2011). The total sigma σ increases from 0.17 at 0.04 s up to 0.24 at longer periods (0.8–1.2 s); τ is about 0.07 over the entire period range, causing the within-event standard deviation to be 95% of the total (see Fig. 16).

5 Conclusions

A predictive model for PGA and 5% damped horizontal spectral acceleration at the period between 0.04 and 4 s is proposed for Iran. Moreover, a regression analysis has been also done to predict vertical to horizontal spectral ratio (V/H) in order to estimate the vertical component of spectrum by scaling horizontal spectra. The models are developed for distances less than 200 km and magnitude between 4 and 7.3, so the applicability of the proposed models is in these ranges. The proposed models are based on the moment magnitude and the Joyner–Boore distance (or the epicentral distance (in km) when the fault geometry is unavailable). In this study, about 1551 free-field acceleration time histories recorded from 200 earthquakes with depth less than 30 km have been used for analyses. The used functional forms include the distance function, the magnitude scaling, the site amplification, and faulting mechanism. The main reason to exclude the nonlinear site amplification effect is that (although we do not reject the existence of soil nonlinearity) we believe that its influence is not strongly apparent in the dataset used in the current study (see also Mousavi et al. 2007), taking into account that most of the dataset do not include recorded PGAs more than 100 gal (Kaklamanos et al. 2013). Moreover, it should be recognized that in the current practice of PSHA in Iran, the hazard analysis is first performed at the bedrock level and then through nonlinear site response analysis, the surface response is evaluated. Seismic building codes also report the design values at the bedrock level. Therefore, taking into account that soil nonlinearity reduces the response levels, it is justifiable to use the proposed GMPEs for PSHA studies in Iran. Finaly, it should be noted that a recent study devoted to test the efficiency of some selected GMPEs against small-to-moderate data recorded in the Iranian plateau, has shown that the model developed in the current study, is the only model that shows good consistency with the recorded data over all frequencies (Zafarani and Farhadi 2017, see also Zafarani and Soghrat 2017b).

Acknowledgements The authors acknowledge the Building and Housing Research Centre of Iran for providing them with the accelerograms and shear wave velocities used in the current study. H. Zafarani and M.R. Soghrat were supported by the International Institute of Earthquake Engineering and Seismology (IIEES) funds. This work has been also supported by the Iran National Science Foundation (INSF).

Appendix

Table 1 Regression coefficients for PGA and pseudo-spectral acceleration (PSA) obtained from geometrical mean of horizontal component (GeoH)

IMs*	M_h†	e_1‖	b_1‖	b_2‖	b_3‖	c_1‖	h‡ (km)
SA (T = 0.04 s)	5.0	3.065	0.491	0.043	0.237	− 1.027	6.835
PSA (T = 0.07 s)	5.3	3.473	0.241	− 0.153	0.204	− 1.137	8.311
PSA (T = 0.1 s)	5.4	3.673	0.283	− 0.116	0.180	− 1.159	9.376
PSA (T = 0.15 s)	5.6	3.623	0.249	− 0.097	0.183	− 1.090	10.228
PSA (T = 0.2 s)	5.8	3.401	0.193	− 0.124	0.207	− 0.963	8.195
PSA (T = 0.25 s)	5.9	3.429	0.227	− 0.112	0.232	− 0.986	11.315
PSA (T = 0.3 s)	6.0	3.383	0.245	− 0.118	0.227	− 0.959	11.012
PSA (T = 0.35 s)	6.0	3.325	0.305	− 0.104	0.241	− 0.947	11.250
PSA (T = 0.4 s)	6.1	3.148	0.277	− 0.128	0.254	− 0.861	7.953
PSA (T = 0.45 s)	6.1	3.089	0.286	− 0.140	0.262	− 0.848	7.498
PSA (T = 0.5 s)	6.2	3.085	0.287	− 0.139	0.263	− 0.847	7.525

Table 1 (continued)

IMs*	M_h†	e_1‖	b_1‖	b_2‖	b_3‖	c_1‖	h‡ (km)	
PSA (T = 0.6 s)	6.3	3.029	0.311	− 0.139	0.277	− 0.836	6.723	
PSA (T = 0.7 s)	6.4	2.926	0.280	− 0.157	0.302	− 0.803	4.967	
PSA (T = 0.8 s)	6.4	2.873	0.317	− 0.159	0.330	− 0.798	4.966	
PSA (T = 0.9 s)	6.5	2.838	0.303	− 0.164	0.373	− 0.787	4.973	
PSA (T = 1 s)	6.5	2.791	0.341	− 0.161	0.372	− 0.782	4.975	
PSA (T = 1.2 s)	6.6	2.738	0.397	− 0.145	0.388	− 0.776	4.976	
PSA (T = 1.4 s)	6.7	2.691	0.442	− 0.128	0.377	− 0.769	4.980	
PSA (T = 1.6 s)	6.7	2.640	0.511	− 0.110	0.410	− 0.777	4.981	
PSA (T = 1.8 s)	6.8	2.642	0.558	− 0.091	0.395	− 0.778	4.994	
PSA (T = 2 s)	6.8	2.600	0.631	− 0.072	0.397	− 0.772	5.001	
PSA (T = 2.5 s)	6.9	2.665	0.789	− 0.026	0.135	− 0.795	6.960	
PSA (T = 3 s)	7.0	2.697	0.851	− 0.008	− 0.062	− 0.809	8.447	
PSA (T = 4 s)	7.2	2.626	0.877	0.001	− 0.455	− 0.775	8.296	
PGA	5.0	2.880	0.554	0.103	0.244	− 0.960	7.283	
	f_{SS}‖	f_{TF}‖	s_B‖	s_C‖	s_D‖	τ**	ϕ**	σ**
PSA (T = 0.04 s)	− 0.023	− 0.045	0.010	− 0.003	− 0.039	0.098	0.294	0.310
PSA (T = 0.07 s)	− 0.014	− 0.046	− 0.006	− 0.037	− 0.055	0.113	0.298	0.319
PSA (T = 0.1 s)	− 0.024	− 0.056	0.007	− 0.052	− 0.049	0.115	0.305	0.326
PSA (T = 0.15 s)	− 0.020	− 0.028	0.061	− 0.001	− 0.029	0.105	0.315	0.332
PSA (T = 0.2 s)	0.001	0.000	0.071	0.022	0.000	0.103	0.309	0.326
PSA (T = 0.25 s)	0.006	0.013	0.080	0.073	0.031	0.102	0.306	0.323
PSA (T = 0.3 s)	− 0.008	0.010	0.073	0.104	0.048	0.103	0.308	0.325
PSA (T = 0.35 s)	− 0.012	0.008	0.073	0.113	0.065	0.103	0.310	0.326
PSA (T = 0.4 s)	− 0.016	0.010	0.076	0.114	0.077	0.104	0.313	0.330
PSA (T = 0.45 s)	− 0.022	0.011	0.074	0.112	0.097	0.104	0.312	0.329
PSA (T = 0.5 s)	− 0.013	0.020	0.060	0.095	0.100	0.104	0.313	0.330
PSA (T = 0.6 s)	− 0.002	0.021	0.056	0.086	0.115	0.106	0.318	0.335
PSA (T = 0.7 s)	0.017	0.031	0.047	0.076	0.133	0.107	0.321	0.338
PSA (T = 0.8 s)	0.017	0.032	0.047	0.065	0.144	0.108	0.323	0.341
PSA (T = 0.9 s)	0.016	0.035	0.043	0.059	0.142	0.108	0.324	0.341
PSA (T = 1 s)	0.022	0.041	0.034	0.056	0.146	0.108	0.325	0.342
PSA (T = 1.2 s)	0.040	0.048	0.038	0.056	0.139	0.108	0.324	0.341
PSA (T = 1.4 s)	0.062	0.059	0.039	0.054	0.135	0.109	0.327	0.345
PSA (T = 1.6 s)	0.077	0.065	0.040	0.058	0.116	0.110	0.329	0.347
PSA (T = 1.8 s)	0.078	0.068	0.047	0.062	0.114	0.109	0.327	0.344
PSA (T = 2 s)	0.077	0.066	0.051	0.065	0.098	0.107	0.322	0.339
PSA (T = 2.5 s)	0.086	0.054	0.053	0.056	0.078	0.104	0.311	0.328
PSA (T = 3 s)	0.099	0.048	0.047	0.041	0.043	0.101	0.303	0.319
PSA (T = 4 s)	0.107	0.023	0.048	0.025	0.032	0.134	0.290	0.319
PGA	− 0.030	− 0.039	0.027	0.010	− 0.017	0.094	0.283	0.298

* IMs—Intensity measures

† M_h—Hinge magnitude

‖ Regression coefficients

‡ h—Pseudo-depth

** Inter-event, intra-event, and total standard deviations

Table 2 Regression coefficients for PGA and pseudo-spectral acceleration obtained for the vertical-to-horizontal ratio (V/H)

IMs*	M_h†	e_1‖	b_1‖	b_2‖	b_3‖	c_1‖	h (km)	
V/H (T = 0.04 s)	5.0	0.215	0.022	0.037	0.021	− 0.257	6.679	
V/H (T = 0.07 s)	5.3	0.153	0.116	0.071	0.032	− 0.195	7.182	
V/H (T = 0.1 s)	5.4	− 0.133	− 0.023	− 0.018	0.041	− 0.093	5.187	
V/H (T = 0.15 s)	5.6	− 0.194	0.016	− 0.001	0.061	− 0.073	7.047	
V/H (T = 0.2 s)	5.8	− 0.196	0.048	0.014	0.041	− 0.072	5.152	
V/H (T = 0.25 s)	5.9	− 0.176	0.075	0.032	0.038	− 0.067	5.136	
V/H (T = 0.3 s)	6.0	− 0.118	0.058	0.009	0.040	− 0.082	5.130	
V/H (T = 0.35 s)	6.0	− 0.113	0.058	0.012	0.043	− 0.080	5.136	
V/H (T = 0.4 s)	6.1	− 0.096	0.070	0.019	0.018	− 0.082	5.142	
V/H (T = 0.45 s)	6.1	− 0.090	0.058	0.010	0.027	− 0.082	6.776	
V/H (T = 0.5 s)	6.2	− 0.083	0.048	0.000	0.017	− 0.079	5.152	
V/H (T = 0.6 s)	6.3	− 0.168	− 0.017	− 0.024	0.015	− 0.046	6.935	
V/H (T = 0.7 s)	6.4	− 0.181	− 0.016	− 0.021	0.025	− 0.030	7.434	
V/H (T = 0.8 s)	6.4	− 0.174	− 0.014	− 0.021	0.005	− 0.024	7.562	
V/H (T = 0.9 s)	6.5	− 0.159	0.016	− 0.006	− 0.027	− 0.019	7.186	
V/H (T = 1 s)	6.5	− 0.157	0.020	− 0.001	− 0.022	− 0.022	7.448	
V/H (T = 1.2 s)	6.6	− 0.158	0.002	− 0.004	− 0.020	− 0.029	7.518	
V/H (T = 1.4 s)	6.7	− 0.112	− 0.001	− 0.009	0.001	− 0.044	12.481	
V/H (T = 1.6 s)	6.7	− 0.120	− 0.004	− 0.011	0.016	− 0.041	13.310	
V/H (T = 1.8 s)	6.8	− 0.113	− 0.005	− 0.011	− 0.027	− 0.037	12.995	
V/H (T = 2 s)	6.8	− 0.117	0.006	− 0.005	− 0.052	− 0.035	13.411	
V/H (T = 2.5 s)	6.9	− 0.184	0.011	0.000	− 0.004	0.011	12.964	
V/H (T = 3 s)	7.0	− 0.188	0.023	0.005	− 0.052	0.020	11.714	
V/H (T = 4 s)	7.2	− 0.212	0.014	0.005	− 0.232	0.036	12.426	
V/H (at PGA)	5.0	− 0.058	0.054	0.098	0.021	− 0.140	6.107	
	f_{SS}‖	f_{TF}‖	s_B‖	s_C‖	s_D‖	τ^{**}	ϕ^{**}	σ^{**}
V/H (T = 0.04 s)	0.021	0.000	0.018	0.016	− 0.017	0.059	0.177	0.186
V/H (T = 0.07 s)	− 0.014	− 0.023	0.056	0.030	0.013	0.062	0.185	0.195
V/H (T = 0.1 s)	0.022	0.020	0.075	0.097	− 0.007	0.064	0.192	0.203
V/H (T = 0.15 s)	0.000	0.007	0.001	0.087	0.012	0.070	0.209	0.221
V/H (T = 0.2 s)	0.008	0.012	− 0.051	0.046	− 0.021	0.067	0.200	0.210
V/H (T = 0.25 s)	− 0.022	− 0.017	− 0.070	− 0.018	− 0.034	0.067	0.201	0.212
V/H (T = 0.3 s)	− 0.033	− 0.031	− 0.082	− 0.093	− 0.050	0.067	0.201	0.212
V/H (T = 0.35 s)	− 0.027	− 0.025	− 0.092	− 0.122	− 0.049	0.068	0.204	0.215
V/H (T = 0.4 s)	− 0.021	− 0.019	− 0.093	− 0.139	− 0.046	0.068	0.204	0.216
V/H (T = 0.45 s)	− 0.029	− 0.015	− 0.090	− 0.151	− 0.068	0.069	0.207	0.218
V/H (T = 0.5 s)	− 0.028	− 0.021	− 0.083	− 0.143	− 0.078	0.069	0.208	0.219
V/H (T = 0.6 s)	− 0.006	− 0.006	− 0.073	− 0.131	− 0.081	0.071	0.213	0.225
V/H (T = 0.7 s)	− 0.008	− 0.005	− 0.078	− 0.126	− 0.117	0.074	0.221	0.233
V/H (T = 0.8 s)	− 0.011	− 0.003	− 0.078	− 0.125	− 0.140	0.075	0.224	0.236
V/H (T = 0.9 s)	− 0.026	− 0.009	− 0.073	− 0.111	− 0.141	0.075	0.225	0.237
V/H (T = 1 s)	− 0.016	0.001	− 0.073	− 0.112	− 0.150	0.075	0.225	0.237
V/H (T = 1.2 s)	− 0.001	0.034	− 0.083	− 0.102	− 0.138	0.074	0.223	0.235
V/H (T = 1.4 s)	− 0.012	0.034	− 0.085	− 0.101	− 0.126	0.073	0.220	0.232

Table 2 (continued)

IMs*	M_h†	e_1‖	b_1‖	b_2‖	b_3‖	c_1‖	h (km)	
V/H (T = 1.6 s)	− 0.007	0.044	− 0.073	− 0.087	− 0.114	0.073	0.220	0.232
V/H (T = 1.8 s)	− 0.011	0.038	− 0.067	− 0.089	− 0.125	0.073	0.220	0.232
V/H (T = 2 s)	− 0.002	0.040	− 0.063	− 0.090	− 0.098	0.073	0.220	0.232
V/H (T = 2.5 s)	0.008	0.050	− 0.065	− 0.089	− 0.081	0.070	0.209	0.220
V/H (T = 3 s)	0.007	0.055	− 0.057	− 0.084	− 0.047	0.069	0.207	0.218
V/H (T = 4 s)	0.000	0.047	− 0.064	− 0.082	− 0.028	0.074	0.223	0.235
V/H (at PGA)	0.005	0.006	0.009	0.033	− 0.019	0.056	0.169	0.179

* IMs—Intensity measures

† M_h—Hinge magnitude

‖ Regression coefficients

‡ h—pseudo-depth

** Inter-event, intra-event, and total standard deviations

References

Abrahamson NA, Youngs RR (1992) A stable algorithm for regression analysis using the random effects model. Bull Seism Soc Am 82:505–510

Akkar S, Bommer JJ (2010) Empirical equations for the prediction of PGA, PGV and spectral accelerations in Europe, the Mediterranean Region and the Middle East. Seism Res Lett 81:195–206

Akkar S, Cagnan Z (2010) A local ground-motion predictive model for Turkey, and its comparison with other regional and global ground-motion models. Bull Seismol Soc Am 100:2978–2995

Akkar S, Sandıkkaya MA, Bommer JJ (2014) Empirical ground-motion models for point-and extended-source crustal earthquake scenarios in Europe and the Middle East. Bull Earthq Eng 12:359–387

Al Atik L, Abrahamson N, Bommer JJ, Scherbaum F, Cotton F, Kuehn N (2010) The variability of ground-motion prediction models and its components. Seismol Res Lett 81:794–801

Ambraseys NN, Douglas J, Sarma SK, Smit PM (2005) Equations for the estimation of strong ground motion from shallow crustal earthquakes using data from Europe and the Middle East: horizontal peak ground acceleration and spectral acceleration. Bull Earthq Eng 3:1–53

Ansari A, Noorzad A, Zafarani H, Vahidifard H (2010) Correction of highly noisy strong motion records using a modified wavelet de-noising method. Soil Dyn Earthq Eng 30:1168–1181

Berberian M (1976) Contribution to the seismotectonics of Iran (Part 2). Geological Survey of Iran Report 39 518pp

Berberian M, Qorashi M, Jackson JA, Priestley K, Wallace T (1992) The Rudbar-Tarom earthquake of 20 June 1990 in NW Persia: preliminary field and seismological observations, and its tectonic significance. Bull Seism Soc Am 82:1726–1755

Beyer K, Bommer JJ (2006) Relationships between median values and between aleatory variabilities for different definitions of the horizontal component of motion. Bull Seism Soc Am 96:1512–1522

Bindi D, Pacor F, Luzi L, Puglia R, Massa M, Ameri G, Paolucci R (2011) Ground motion prediction equations derived from the Italian strong motion database. Bull Seism Soc Am 9:1899–1920

Bindi D, Massa M, Luzi L, Ameri G, Pacor F, Puglia R, Augliera P (2014) Pan-European ground-motion prediction equations for the average horizontal component of PGA, PGV, and 5%-damped PSA at spectral periods up to 3.0 s using the RESORCE dataset. Bull Earthq Eng 12:391–430

Bommer JJ, Douglas J, Scherbaum F, Cotton F, Bungum H, Fah D (2010) On the selection of ground-motion prediction equations for seismic hazard analysis. Seism Res Lett 81:783–793

Bommer JJ, Akkar S, Kale O (2011) A model for vertical-to-horizontal response spectral ratios for Europe and the Middle East. Bull Seism Soc Am 101:1783–1806

Boore DM, Atkinson G (2008) Ground motion prediction equations for the average horizontal component of PGA, PGV, and 5%-damped PSA at spectral periods between 0.01 s and 10.0 s. Earthquake Spect 24:99–138

Boore DM, Stewart JP, Seyhan E, Atkinson GM (2014) NGA-West2 equations for predicting PGA, PGV, and 5% damped PSA for shallow crustal earthquakes. Earthq Spectra 30(3):1057–1085

Bozorgnia Y, Campbell KW (2004) The vertical-to-horizontal response spectral ratio and tentative procedures for developing simplified V/H and vertical design spectra. J Earthq Eng 8:175–207

Budnitz RJ, Apostolakis G, Boore DM, Cluff LS, Coppersmith K, Cornell CA, Morris BJ (1997) Recommendations for probabilistic seismic hazard analysis, in guidance on uncertainty and use of experts. Lawrence Livermore National Laboratory, Vol. 2. US Nuclear Regulatory Commission, Rockville, MD

Cotton F, Scherbaum F, Bommer JJ, Bungum H (2006) Criteria for selecting and adjusting ground-motion models for specific target applications: applications to Central Europe and rock sites. J Seismol 10:137–156

Delavaud E, Scherbaum F, Kuehn N, Allen T (2012) Testing the global applicability of ground-motion prediction equations for active shallow crustal regions. Bull Seismol Soc Am 102: 707–721

Douglas J (2011) Ground-motion prediction equations 1964–2010, Final Rept. RP-59356-FR, Bureau de Recherches Géologiques et Minières (BRGM), Orléans, France, 444 pp.

European Committee for Standardization, CEN (2003) Eurocode 8: design of structures for earthquake resistance—part 1: general rules, seismic actions and rules for buildings, EN-1998-1: 2003. European Committee for Standardization, Brussels

Ghasemi H, Zare M, Fukushima Y, Koketsu K (2009a) An empirical spectral ground-motion model for Iran. J Seismol 13: 499–515

Ghasemi H, Zare M, Fukushima Y, Sinaeian F (2009b) Applying empirical methods in site classification, using response spectral ratio (H/V): a case study on Iranian strong motion network (ISMN). Soil Dyn Earthq Eng 29:121–132

Gregor N, Abrahamson NA, Atkinson GM, Boore DM, Bozorgnia Y, Campbell KW et al (2014) Comparison of NGA-West2 GMPEs. Earthq Spec 30(3):1179–1197

Halldorsson B, Papageorgiou AS (2005) Calibration of the specific barrier model to earthquakes of different tectonic regions. Bull Seis Soc Am 95:1276–1300

Jahanandish M, Zafarani H, Shafiee AH (2017) Implementation of the square-root-impedance method to estimate site amplification in Iran using random profile generation. Bull Seis Soc Am 107:456–467

Kaklamanos J, Baise LG, Boore DM (2011) Estimating unknown input parameters when implementing the NGA groundmotion prediction equations in engineering practice. Earthq Spectra 27:1219–1235

Kaklamanos J, Bradley BA, Thompson EM, Baise LG (2013) Critical parameters affecting bias and variability in site-response analyses using KiK-net downhole array data. Bul Seisl Soc Am 103:1733–1749

Kale Ö, Akkar S, Ansari A, Hamzehloo H (2015) A ground-motion predictive model for Iran and Turkey for horizontal PGA, PGV, and 5%-damped response spectrum: investigation of possible regional effects. Bull Seismol Soc Am 105: 963–980

Khodaverdian A, Zafarani H, Rahimain M (2015) Long term fault slip rates, distributed deformation rates and forecast of seismicity in the Iranian Plateau. Tectonics 34:2190–2220

McGuire RK (1978) Frisk: computer program for seismic risk analysis using faults as earthquake sources. United States Department of the Interior, Geological Survey, Open-File Report, 78–107

Mirzaei N, Gao M, Chen YT (1998) Seismic source regionalization for seismic zoning of Iran: major seismotectonic Provinces. Journal of Earthquake Prediction Research 7: 465–495

Mousavi M, Zafarani H, Noorzad A, Ansari A, Bargi K (2007) Analysis of Iranian strong-motion data using the specific barrier model. J Geophys Eng 4:415–428

Mousavi M, Zafarani H, Rahpeyma S, Azarbakht A (2014) Test of goodness of the NGA ground-motion equations to predict the strong motions of the 2012 Ahar-Varzaghan dual earthquakes in northwestern Iran. Bull Seism Soc Am 104:2512–2528

Mousavi M, Ansari A, Zafarani H, Azarbakht A (2012) Selection of ground motion prediction models for seismic hazard analysis in the Zagros Region, Iran. J Earthq Eng 16:1184–1207

Musson RMW (2009) Ground motion and probabilistic hazard. Bull Earthq Eng 7:575–589

Niazi M, Bozorgnia Y (1992) The 1990 Manjil, Iran, earthquake: geology and seismology overview, PGA attenuation, and observed damage. Bull Seismol Soc Am 82:774–799

Nowroozi AA (1976) Seismotectonic provinces of Iran. Bull Seismol Soc Am 66:1249–1276

Power M, Chiou B, Abrahamson N, Bozorgnia Y, Shantz T, Roblee C (2008) An overview of the NGA project. Earthq Spect 24:3–21

Saffari H, Kuwata Y, Takada S, Mahdavian A (2012) Updated PGA, PGV, and spectral acceleration attenuation relations for Iran. Earthq Spect 28:257–276

Scasserra G, Stewart JP, Bazzurro P, Lanzo G, Mollaioli F (2009) A comparison of NGA ground-motion prediction equations to Italian data. Bull Seismol Soc Am 99:2961–2978

Shahvar MP, Zare M, Castellaro S (2013) A unified seismic catalog for the Iranian plateau (1900–2011). Seismol Res Lett 84:233–249

Scherbaum F, Cotton F, Smit P (2004) On the use of response spectral-reference data for the selection and ranking of ground motion models for seismic-hazard analysis in regions of moderate seismicity: the case of rock motion. Bull Seismol Soc Am 94(6):2164–2185

Scherbaum F, Delavaud E, Riggelsen C (2009) Model selection in seismic hazard analysis: an information-theoretic perspective. Bull Seismol Soc Am 99(6):3234–3247

Shoja-Taheri J, Anderson JG (1988) The 1978 Tabas, Iran, earthquake: an interpretation of the strong-motion records. Bull Seismol Soc Am 78:142–171

Soghrat MR, Khaji N, Zafarani H (2012) Simulation of strong ground motion in northern Iran using the specific barrier model. Geophys J Int 188:645–679

Soghrat MR, Ziyaeifar M (2016) A predictive equation for vertical-to-horizontal response spectral ratios in Northern Iran. Bull Seis Soc Am 106:123–140

Takin M (1972) Iranian geology and continental drift in the Middle East. Nature 235:147–150

Trifunac MD, Lee VW (1973) Routine computer processing of strong motion accelerograms. Report EERL 73-03, Calif. Inst. of Tech., Pasadena, California

Zafarani H, Mousavi M, Noorzad A, Ansari A (2008) Calibration of the specific barrier model to Iranian plateau earthquakes and development of physically based attenuation relationships for Iran. Soil Dyn Earthq Eng 28:550–576

Zafarani H, Farhadi A (2017) Testing ground-motion prediction equations against small-to-moderate magnitude data in Iran. Bull Seismol Soc Am 107:912–933

Zafarani H, Soghrat MR (2017a) A selected dataset of the Iranian strong motion records. Nat Hazards 86:1307–1332

Zafarani H, Soghrat MR (2017b) Single-station sigma for the Iranian strong-motion stations. Pure Appl Geophys. https://doi.org/10.1007/s00024-017-1613-z

Zafarani H, Hassani B (2013) Site response and source spectra of S-waves in the Zagros region, Iran. J Seismol 17:645–666

Zafarani H, Mousavi M (2014) Applicability of different ground-motion prediction models for northern Iran. Nat Hazards 73: 1199–1228

Zafarani H, Soghrat MR (2012) Simulation of ground motion in the Zagros region, Iran using the specific barrier model and stochastic method. Bull Seism Soc Am 102:2031–2045

Zafarani H, Hassani B, Ansari A (2012) Estimation of earthquake parameters in the Alborz seismic zone, Iran using generalized inversion method. Soil Dyn Earthq Eng 42:197–218

Zare M, Bard PY, Ghafory-Ashtiany M (1999) Site characterizations for the Iranian strong motion network. Soil Dyn Earthq Eng 18:101–123